HOW TO BUILD HIGH POWER PULSED SUM FREQUENCY LASERS.

Summary

In this report we develop the theory of our pulsed IR lasers and sum frequency conversion techniques and combine the theory with experimental measurements to predict the performance of the existing laser. The theory is then used to investigate ways of reaching higher powers.

(1) Predicting the power and pulse shape of pulsed laser oscillators

(1.1) Theory

The most satisfactory way to calculate the performance of the existing and future lasers is to solve the rate equations that determine the density of photons in the cavity and the population inversion in the gain material. These rate equations depend on the loop gain of the laser and this is made up of three components, the gain of the Nd: YAG slab, cavity losses and the signal dependent losses of the non-linear crystal that damp out the relaxation oscillations.

The logarithmic loop gain of the laser cavity is given by:

$$g = 4 \cdot \sigma \cdot l \cdot n(t) + Log_n\left(T^2 \cdot R\right) + Log_n(1 - a \cdot \phi(t)) \qquad (1)$$

Where σ is the effective stimulated emission cross-section
l is the slab length
n(t) is the population inversion in atoms/cm^3
T is Σ (1- L_i), the sum of the one-way loss of each element in the cavity including diffraction effects
R is the reflectivity of the output coupler
a is the conversion efficiency of the non-linear crystal
ϕ(t) is the photon density in the cavity in photons/cm^3

The factor 4 in the first term comes about because the beam travels through the slab 4 times before returned to its original position.

Each complete cycle through the cavity increases the photon density by a factor of g and reduces the population inversion in proportion. The population inversion is also reduced by losses due to fluorescence and is maintained by photons absorbed from the pump source. This gives rise to two non-linear coupled equations, which can be expressed as two difference equations:

$$\phi[i+1] = \phi[i] + \beta \cdot g \cdot \phi[i] \qquad (2)$$

and $$n[i+1] = n[i] + \beta\left(-2 \cdot \sigma \cdot L \cdot \phi[i] \cdot n[i] + t_c \cdot k1 - n[i] \cdot t_c / \tau_f\right) \quad (3)$$

Where ϕ[i] is the photon density in the cavity on the ith iteration
n[i] is the population inversion in the slab
L is the length of the cavity
t_c is the time to make one cycle through the cavity
τ_f is the fluorescence lifetime
β is the step size in units of t_c

The photon density is constant through the cavity, but really consists of two beams, one traveling left to right, I_+, and the other right to left I_- (see figure 1) Only photons going left to right leave the cavity, so that the output power is given by:

$$P(t) = \frac{1-R}{1+R} \cdot h\nu \cdot c \cdot \eta_i \cdot A_{eff} \quad (4)$$

Where R is the reflectivity of the Output Coupler
hν is the energy of a 1319 nm photon
c is the speed of light
η_I is the interaction efficiency that measures how many atoms available in the slab interact with the laser beam
A_{eff} is the effective area of the laser beam

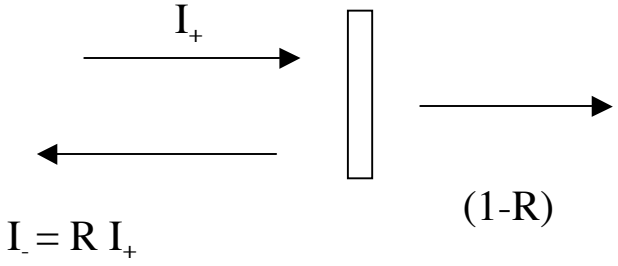

Figure 1: *Calculation of the Intensity of light leaving the cavity*

(1.2) Measurements

To determine the power produced by the laser it is necessary to know:

(1) The power produced by the diode pump lasers
(2) The fraction of this power that gets absorbs by the gain material
(3) The resultant population inversion
(4) The cavity losses
(5) The reflectivity of the output coupler.
(6) The interaction efficiency of the material with the beam.

(7) The effective area of the beam.

We can measure items (1), (5), (6) and (7) experimentally, we have to estimate (2) and (4) and we can calculate (3) using a measured stimulated emission cross-section.

(1.2.1) Laser pump power

Since direct measurement of the individual diode laser modules requires us to physically dismantle the laser, we estimated this number from original power measurements as follows. The two diode laser modules used in 1.32 μ laser were originally measured to give a combined power of 1900 watts of peak power at 110 amps. While we cannot measure the absolute power of each laser module we can determine their relative power by measuring the fluorescence generated by each module operated on its own and we find that one diode module now produces a slab fluorescence 75% less than the other. From this observation, we can set the maximum power level of 1700 watts. Since the diodes have already generated 10^9 pulses a combined power level of no more than 1600 watts seems more realistic, and this value has been adopted in the calculations.

(1.2.2) Fraction of pump light absorbed by Nd: YAG

The amount of pump light absorbed by the Nd:YAG depends on the spectral linewidths of the exciting source. For the LLNL diode laser modules, these line widths lie between 3 nm FWHM and 4 nm FWHM. We have convolved the high-resolution absorption profile of Nd: YAG with both linewidths for laser diode modules operated at a water temperature of 23 ^{O} C. This data is shown in figure 2.

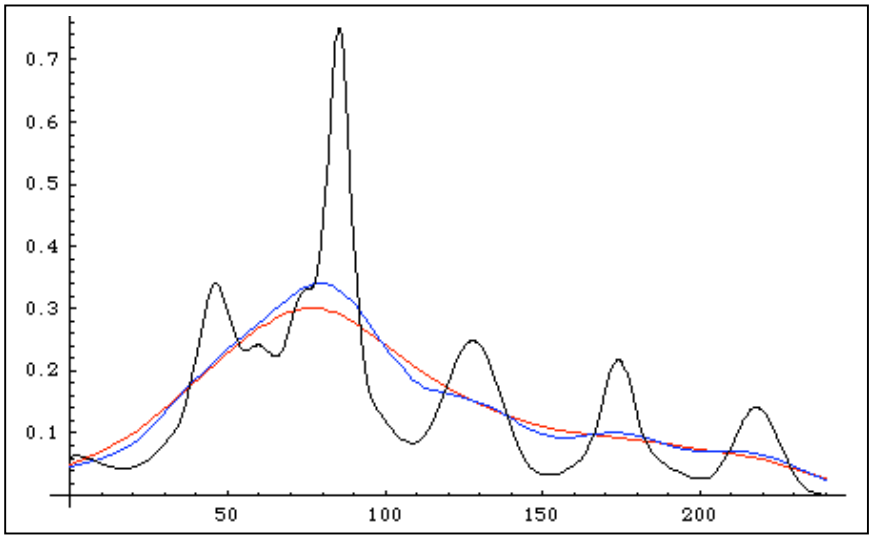

Figure 2: *Absorption spectrum of Nd: YAG from 800 to 820 nm (Black)*
Convolved spectrum with Gaussian 3 nm FWHM (Blue)

Convolved spectrum with Gaussian 4 nm FWHM (Red)
Vertical scale is absorption length in units of cm^{-1}

This data gives us an absorption length of 0.30 cm^{-1} at the peak. Since the slab is 3 mm thick, we expect 59% of the light to be absorbed by the material in a single pass. To improve this efficiency, laser module has a cylindrical mirror on either side of the Nd: YAG slab to redirect the light back into the slab, giving in a theoretical absorption efficiency of 0.82. However, direct measurements show that the retro reflector is less effective than assumed. We estimate that 69% of the diode laser photons are absorbed by the Nd:YAG material.

(1.2.3) Population Inversion

Not all atoms excited to the upper state contribute to the population inversion and the upper state itself is split, only one level contributing to the relevant population inversion. Following general literature [],[], we have assumed that 85% of the excited atoms contribute to the population inversion**.** The gain of the laser depends on the product of the density of excited atoms and a stimulated emission cross-section. There are various definitions and values of this cross-section given in the literature. We have assumed a value of 2.8 x 10^{-19} cm^2 for the 1.064 μ transition and 0.9 x 10^{-19} cm^2 for the 1.319 μ transition.

(1.2.4) Cavity Losses

The output power of the laser is critically dependent on the losses in the cavity. These losses are difficult to estimate ,and we have used the cavity losses as a free parameter in the code, changing the losses to match the output power of the laser. This also corrects for some error in estimating the effective cross-section. It is, however, useful to have an independent estimate of these losses under given conditions. The estimated absorption losses for a single pass (that is for a photon moving from the HR to OC) in the cavity are given below:

TABLE 1

Optical Element	**Transmission**
Fold mirrors 4@ 99.5%	0.98
Acousto-optic modulator	0.99
$LiIO_3$ NLX	0.97
Tuning Etalons	0.97
Lenses @ 99 %	0.98
Two pass absorption in Nd:YAG slab @ 0.003/cm	0.95
TOTAL TRANSMISSION	**0.85**

There are additional losses, due to diffraction in the cavity, caused by surface imperfections, diffraction at the edges of the slab and/or high order thermal distortions of the beam. The edges of the slab present a slit 0.262 cm across the laser beam and introduce a 5% for the TEM_{00} mode. Even though the quality of the optics and coating is very high and the beam is small there are 17 surfaces in the cavity and even a 1/25 wave rms distortion, loses us another 6%, so that the one pass transmission losses of about 75% obtained from the code seem reasonable. More significant are the losses due to high order thermal lensing; these increase with the pump power and ultimately set the maximum power that can be obtained from any given laser. The strongest Zernike components of this distortion are Focus and/or astigmatism, both of which can be corrected by using additional optics in the laser cavity. Thus this type of thermal lensing is not, of itself a limiting factor, although it is also true that the stronger the powers of the lensing the more sensitive the laser becomes to the drive conditions. Higher order aberrations are much harder to correct. The amplitude of these aberrations scale with input power and causes a power loss of Exp[- constant x P^2]. In order to scale our laser to higher powers at is necessity to determine the constant, which we have done in a number of different ways.

(1.2.4.1) Direct Measurement

Viswa and I have already measured the wavefront distortion across the slabs used to the SF laser in the most favorable case in which the diode laser light is distributed uniformly across the slab. The optical layout of the test is shown in figure 3.

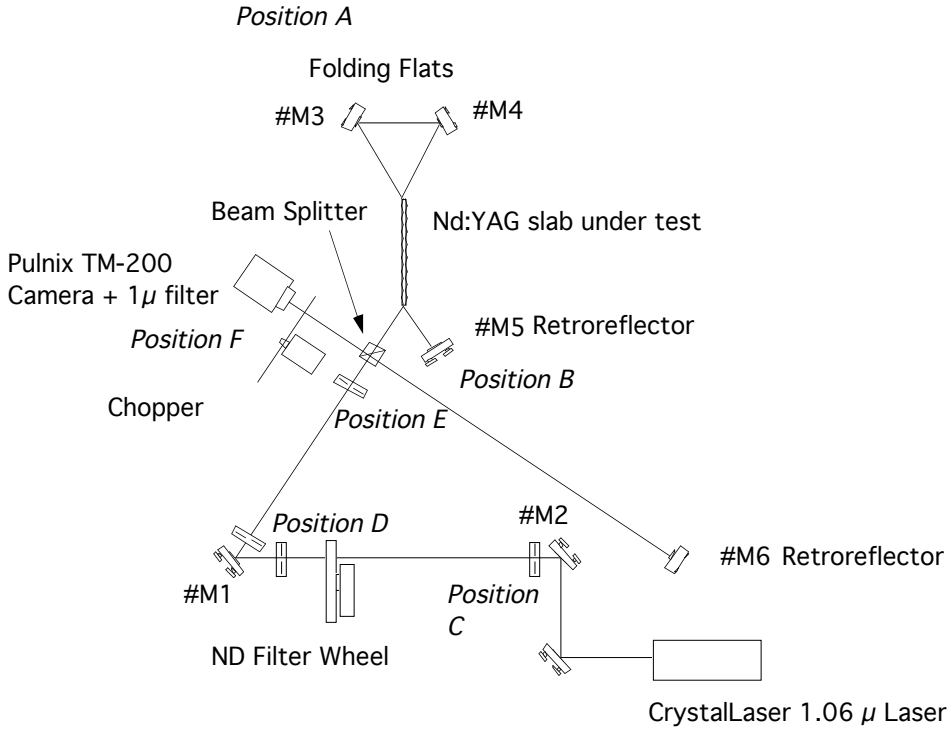

Figure 3: *Optical layout of the Interferometer used to measure the Nd:YAG wavefront errors. The test beam passes through the slab 4 times.*

Thermal lens data from the 1.32 μ slab is shown in figure 4 and represents the curvature and wavefront distortion of a 1.06 μ laser beam passing 4 times through the slab with an input pump power to the slab of 170 watts. The curvature is equivalent to a thermal lens of 3 meters. There is no evidence of higher order Zernike terms in this data and we can say that the amplitude of higher terms is less than 20 nm rms, which is the same order as the measurement error.

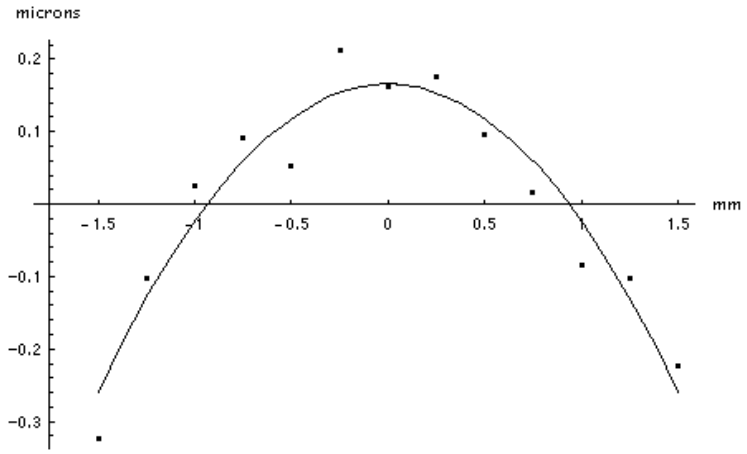

Figure 4: *Wavefront distortion of the 1.32 μ laser slab in the vertical direction.*

(1.2.4.2) Analytical Theory

A Gaussian beam traveling through an absorbing medium changes the temperature of the material and creates a thermal lens with it. In the case of radial symmetry in an infinite slab, we can write the radial temperature distribution, for a normalized $1/e^2$ intensity beam, as an expansion:

$$\Delta T = \sum_{n=1}^{\infty} \frac{-2^n}{n \cdot n!} r^{2 \cdot n} \tag{5}$$

and can calculate an rms wavefront error, weighted with the intensity profile, between this exact temperature profile and the parabolic approximation to this profile. These profiles are shown in figure 5 .

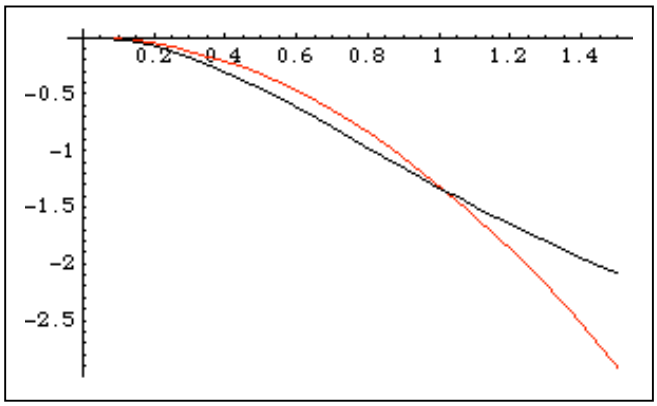

Figure 5 *: The wavefront distortion due to a Gaussian beam is shown in black, together with a parabolic curve representing the best approximation to a parabolic thermal lens.*

We find that the rms wavefront error due to high order wavefront distortions is equal to 0.0751 times the parabolic wavefront distortion between the central of the slab and the $1/e^2$ intensity of the laser beam. However, we also know that , for a rectangular slab with uniform heat deposited throughout the volume and heat removed uniformly from the sides, the temperature distribution is parabolic and high order distortions are very small. Our situation is one in which a quasi-Gaussian beam is focused into an essentially infinite slab and heat removed along the direction of the pump beam; this is an intermediate case and the true value of the scaling factor lies between 0 and 0.0751. We have adopted the value of 0.0751 as the worst case.

(1.2.4.3) Calculation of the effect of thermal lensing on laser performance

The current laser uses a diverging cylindrical lens to correct beam focusing in the vertical direction and the focal length of this lens provides a direct measure of the focal length of the thermal lens. When the laser is operated at 300 Hz with 115 amp 189 μsec drive pulses to the laser we find that we need a cylindrical lens of -40 cm to correct for the thermal lensing in the slab and obtain maximum energy (16.7 mJ/pulse) and a circular near field beam leaving the laser. We use a -25 cm to correct the thermal lensing at 500 Hz and have measured the energy/pulse as 16.2 mJ. The average $1/e^2$ intensity radius of the beam at the slab is 0.076 cm so that the cylindrical lens is correcting a wavefront distortion of 580 nm across the $1/e^2$ beam radius for two passes through the slab. If we assume the thermal profile is given by (5), then high order thermal distortions introduce a wavefront error of 43 nm. This wavefront error introduces a loss that can be described as a one-way effective transmission into the cavity of

$$T_{thermal} = Exp[-\left(2\pi \cdot 43 \cdot P/\left(150 \cdot 1319\right)\right)^2] \qquad (6)$$

Where P is the average power of the diode laser pump.

(1.3) Coupling Efficiency

We can change the focusing of the diode pump light in the slab from about 0.08 cm to 0.2 cm FWHM. The tighter the focusing the better the coupling between the pump light and the TEM_{00} mode of the laser, but the more severe the thermal lensing. Numerical simulation and experiment shows that, if no additional heating is applied to the top and bottom of the slab [2], a FWHM for the focused laser of 0.12 cm is optimum for a mean optical pump power of 200 watts. A photograph of TV camera image looked along the slab is shown in photograph 1, together with photometric traces of the beam with the laser on and off. The strength of fluorescence integrated along the length of the crystal has been measured with a CCD camera with and without laser action. This data is shown in figure 6. The curve on the left represents to subtraction of these two sets of data and represents the amount of fluorescence actually involved in the laser action; the interaction efficiency is defined as the power used by the laser beam/total fluorescent power; 40-45 % of the fluorescent photons couple into the laser beam. The subtracted images give a Gaussian profile with the same FWHM as the laser beam in the slab.

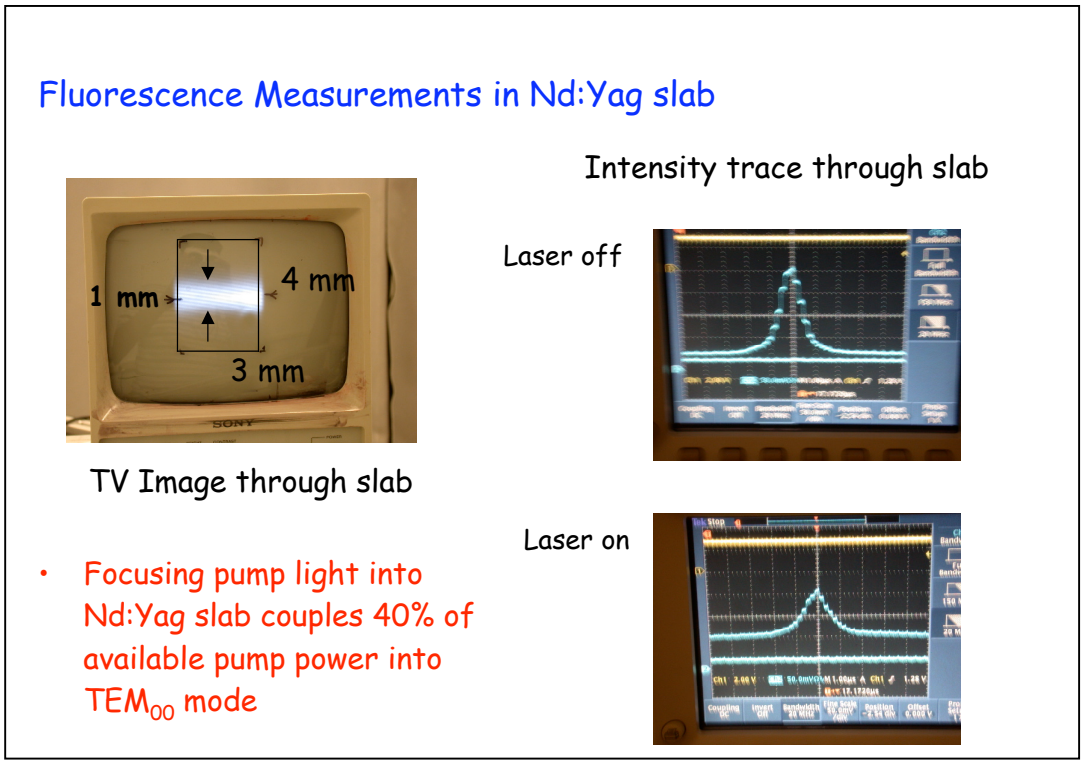

Photograph 1: Measuring the Fluorescence profile of the laser. The left hand image shows the fluorescence through the slab taken with a CCD camera. The images on the right show the output of a line scan CCD measuring the fluorescenec in the vertical direction, integrated across the horizontal axis. Filters were introduced to suppress 1.32 μ light.

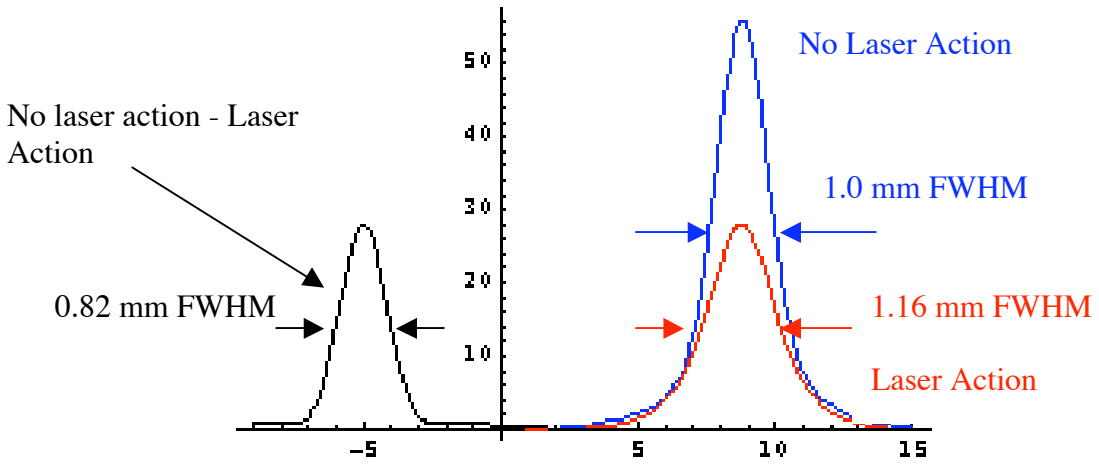

Figure 6: *Fluorescence profiles of the 1.32 μ laser gain engine in the vertical direction*

(1.4) Effective Area of beam

The pump volume of the slab is given by:

$$V = l \cdot w \cdot \sqrt{2\pi} \cdot \left(FWHM/2.35\right) \tag{7}$$

Where l is the length of slab being pumped
w is the thickness of the slab
FWHM is the FWHM width of the pump beam

We have assumed that the effective area of the laser beam is given by :

$$A_{eff} = \eta_i \cdot w \cdot \sqrt{2\pi} \cdot \left(FWHM/2.35\right) \tag{8}$$

Where η_I is the coupling efficiency determined above. This is consistent with the definition of beam overlap efficiency given in Koechner [page 92]

(1..5) Results

The output code gives pulse profile shown in figure for conditions of

Diode Pump power	1600 watts
OC reflectivity	0.7
High order thermal losses	0.04

Single Pass losses expressed as a transmission	0.75
Pulse Width	189 μsec
Rep Rate	500 Hz

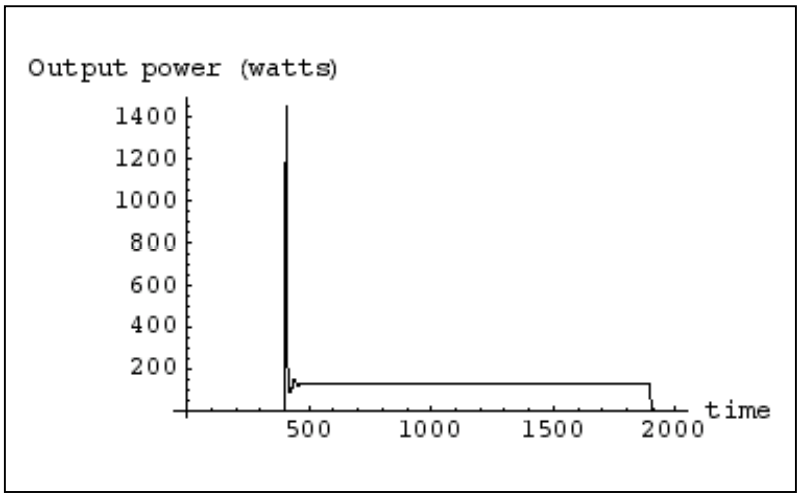

Figure 7. Calculated profile of the 1.32 μ laser

The calculated and measured energies and turn-on times are given below:

	Calculated	Measured
Energy/Pulse	19.78 mJ	19-21 mJ
Turn on time	40.5 μsecond	39-42 μsec
Average power in pulse	219 watts	
Peak Power	1455 watts	

(2) Improvements to the Current 1.32 μ laser

(2.1) Reducing Losses within the cavity

We are now in a position to optimize the output power of the laser. Figure 8 shows the effect of losses in the cavity. The effect of changing the losses in the cavity under current conditions is shown in figure 8.

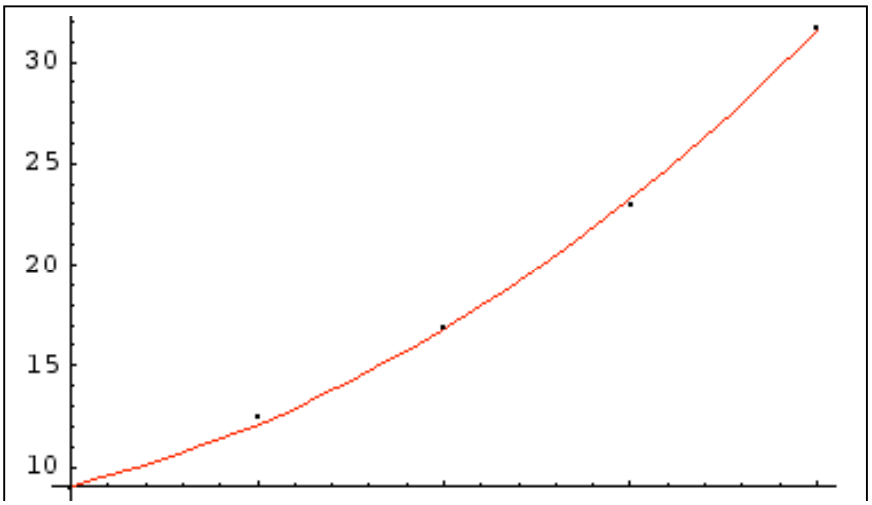

***Figure 8**: Calculated Energy/pulse as a function of Cavity Transmission (1pass-Loss) For OC Reflectivity of 0.7*

This figure shows the advantage of reduces losses in the cavity. The optics are already chosen for low losses but replacing the NLX and etalons (inherited from the MIT/LL prototype laser) might provide some gain in output power.

(2.2) Changing the Reflectivity of the Output Coupler

We show the effect of changing the reflectivity in figure 9. We tested an Output Coupler with a Reflectivity of 0.54 that was used in September 2004. The measured laser output was 16.3 mJ /pulse at R=0.7 and 18.8 mJ at R = 0.54 with turn on delays of 42 μsec and 52 μsec respectively. The improvement in output power (15%) was offset by an increased sensitivity to scattered light return from the SFC when operated mode-locked so we went back to the 70% reflection OC. The increase the output is lower than that predicted by the code. This may be because we not have an accurate measurement of the output coupler -a reflectivity of 0.65 would make the original data consistent. We have improved our alignment procedures and the gain of the laser is higher than in 2004 so we may expect a 10-20% increase in power going to a lower OC reflectivity.

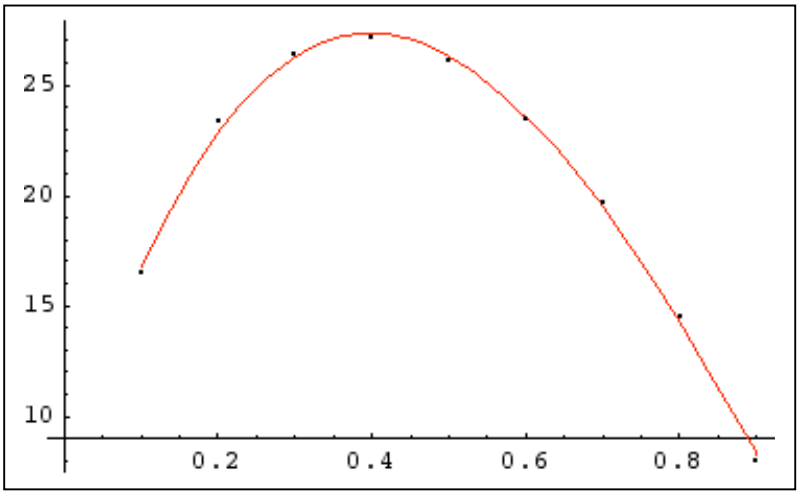

***Figure 9:** Energy/pulse as a function of Output Coupler Reflectivity*

(2.3) Adjusting the lengths of the micropulses

At present we are limited by the output power of the drive amplifiers. The power rating of the driver is proportional to current x pulse width (the voltage is fixed across the diodes). We can change the current and pulse width together to stay within the power rating of the drivers, shorter pulses can have higher currents. The effect of changing the pulsewisth within this constraint is shown in figure 10.

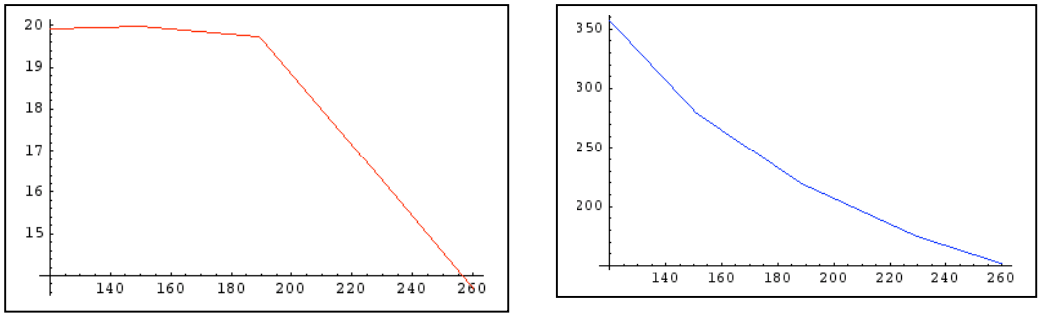

Figure 10: *(a) Energy/pulse as a function of pulse width in µsec (Red)*
(b) Power within pulse as a function of pulse width in µsec (Blue)

These plots show that while there is little gain in the energy/pulse going to shorter pulses, there is some gain in the pulse power and this will be reflected in conversion efficiency in the SFC. Shorter pulses are probably not a good idea if we mode lock since there is an appreciable delay in attaining a stable mode-lock pulse train. Shorter pulses will help if we use PPSLT material, provided we don't blow the material up.

(2.4) Going to Higher Rep Rates.

If we use higher power drivers, we can maintain the same pulse width and pump power as we increase the operating frequency and obtain more power from the laser. The laser energy/pulse falls because the extra heat load increases the losses inside the cavity. The energy /pulse is shown as a function of rep rate in figure 11 for the one head and two head case.

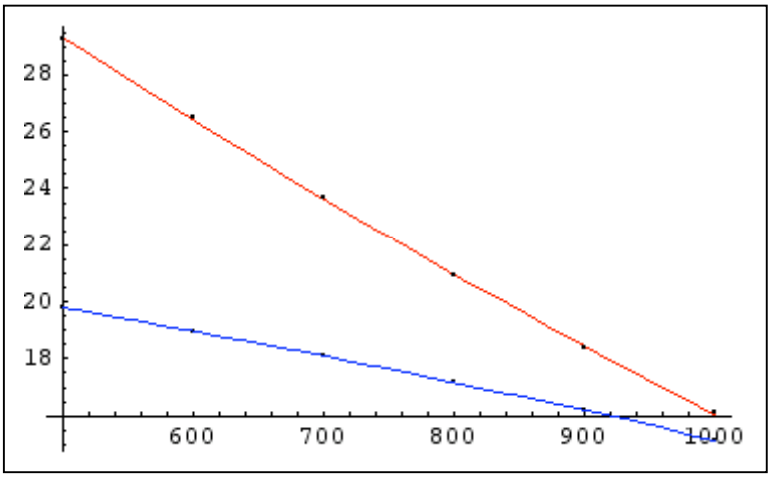

Figure 11: *Energy/pulse as a function of rep rate for current laser parameters assuming 43 nm rms error front error due to high order thermal lensing at 500 Hz.*
Single head (blue), Double Head (red)

These curves show the significant loss in energy/pulse at high rep rates due to losses from high order thermal distortions. As noted previously, the wavefront error assumed in these calculations may be pessimistic. Figure 12 shows a more optimistic case in which the wavefront error is half this value (22.5 nm). Even small improvements in beam quality (such as could be obtained using aspherical components) could make a difference in overall power at high rep rates.

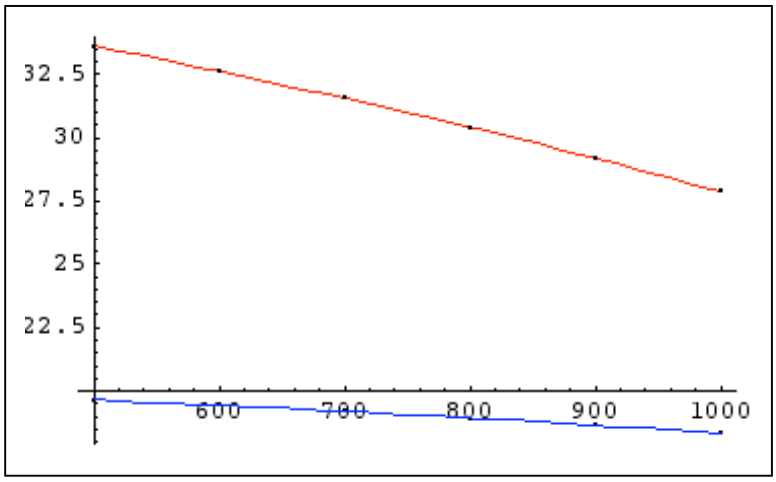

Figure 12*: Energy/pulse as a function of rep rate for current laser parameters Assuming 21.5 nm rms error front error due to high order thermal lensing at 500 Hz. Single head (blue), Double Head (red)*

This data shows the importance of controlling high order thermal lensing and/or using a double head at kHz rep rates.

(2.5) Building new heads

(2.5.1) Thermal Control

We have carried out a simulation of the thermal profile for a 1 mm FWHM laser diode beam focused in the slab and 40% heat transfer into the Nd:YAG. Heat is removed from the slab via sapphire slabs into a copper heat sink and this is modeled in the code. The thermal profile of the Nd:YAG with no heat removal from the top and bottom of the slab is shown in figure 13 . Because we use a zigzag slab configuration, the effect of thermal gradients are zero to first order on the horizontal component of the laser beam; we have therefore integrated along the horizontal direction and display the temperature above coolant as a function of height in the vertical direction in figure 13c. Also shown is the

thermal profile when heat is introduced at the top and bottom surfaces to minimize the thermal lens.

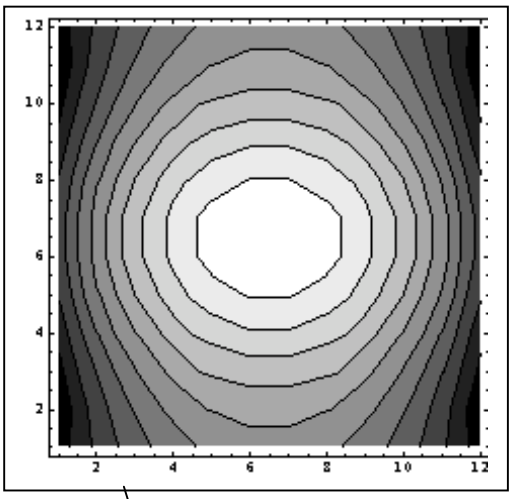

Figure 13a

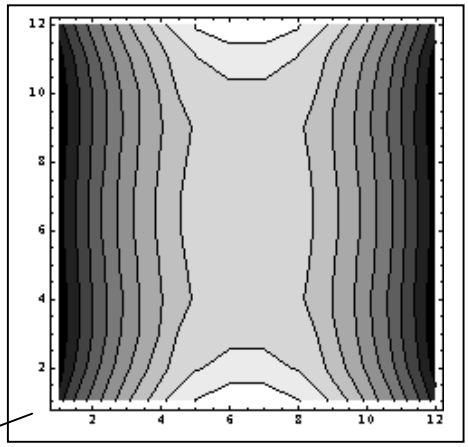

Figure 13b

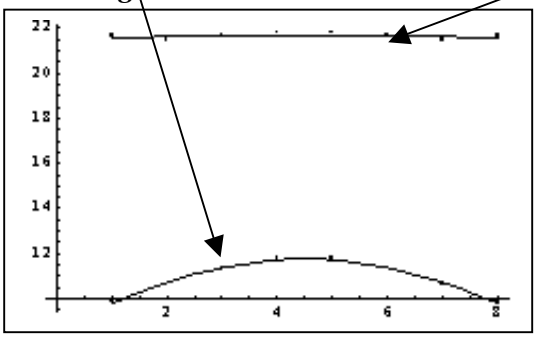

Figure 13c

Figure 13a: *Computed temperature profiles for current 1.32 μ laser.*

13b: *Computed temperature profiles for identical laser with heaters.*

13c*: Vertical temperature profiles integrated horizontally for the two cases*

Heat generation and removal is critical for efficient operation of the laser and the Physics of the laser is more complex that suggested by the code. The Nd:YAG slab strongly absorbs the diode laser pump light to level 4. The Nd atoms relax to Level 3 via non- radiative (phonon) transitions then cascade to the ground state via photon and phonon transitions. For a given laser transition of λ_L ,the minimum fraction of power dumped into the YAG material is given by the Stokes loss $(\nu_{808} - \nu_L)/\nu_{808}$. Because some sites are non-radiative [] and there can be substantial up-conversion [] the heat load depends on other factors and especially whether the material is lasing or not. Photons not taking part in stimulated emission are either absorbed by the Copper heat exchanger, reabsorbed by the Nd:YAG, or diffuse out of the slabs and these interactions complicate the calculation of the heat distribution within the slab. When the laser is not operating about 7% of the heat is given out by the laser diode photons going from state 4 to 3 and about 15% of the heat is generated by fluorescence decay and phonon transitions to the

ground level and about 10% of the heat is generated from non-radiative sites to level 3. This distribution in heat is proportional to the intensity of the diode laser beam. When the laser is operating, the excited atoms in the beam are stimulated to go directly from state 3 to 2 and thence via phonon transitions to the ground state. For the 1.064 transition, this results in a decrease in heat into the material within the laser beam, for 1.32 μ the heat input is greater. Laser action therefore gives rise to an additional spherical lens that is negative for the 1.06 μ transition and positive for the 1.32 μ transition. An exact calculation of the thermal lens requires us to introduce all of these interactions into the model.

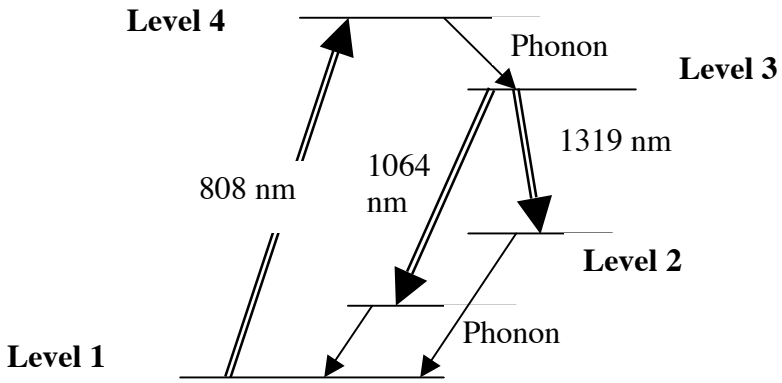

Figure 14: Energy States of Nd:YAG

We can however make some general comments about thermal lensing in the slab:

(1) For a pump beam with a Gaussian intensity profile, amount of high order thermal lensing seems always to be smaller than that predicted by equation xx.

(2) Introduction of heat at the top and bottom surfaces can reduce the thermal lensing of the slab []. This is shown in figure xx.

(3) Introduction of this heat does not necessarily reduce high order thermal lensing and, if anything, makes it worse.

(4) The slab is transparent to most of the fluorescent light so that a significant fraction of the photons not taking part in the laser action either leave the slab and are absorbed by the copper cooling blocks, are reabsorbed by the material or diffuse out of the slab via the sapphire heat sinks. This redistribution of heat is difficult to model and further complicates a theoretical determination of the heat distribution within the slab.

We have designed the new gain engines that can provide heat input into the top and bottom of the slabs. As noted above, this does not reduce, and may increase, high order

wavefront distortions and the effect of parabolic wavefront distortion can be taken out with suitable lenses inserted into the laser cavity. The importance of providing heating to the slab is that we can control the total thermal lensing of the slab throughout the lifetime of the laser. When operating at kHz rep rates, we intend to use a -15 cm lens to take out a major fraction of the thermal lens and to regulate the heat input to stabilize the focus of the slab to an optimum length.

(2.5.2) Predicted Performance of lasers

(2.5.2.1) 1.32 μ laser

A summary of the Energy/pulse at different rep rates is given in Table 2. The cavity losses have been adjusted to give 19.8 mJ @ 500 Hz in the single head. We believe the thermal losses are better than 43nm but worse than 21.5 nm; our best guess,based on experimental data, is 38nm.

TABLE 2

Rep Rate	**Single Head 43 nm@ 500 Hz**	**Single Head 21.5 nm@ 500 Hz**	**Double Head 43 nm**	**Double Head 21.5 nm**
500 Hz	19.8 mJ	19.8 mJ	29.3 mJ	35.6 mJ
800 Hz	17.2 mJ	19.0 mJ	21.0 mJ	30.4 mJ
1000 Hz	15.2 mJ	18.3 mJ	16.1 mJ	27.9 mJ

(2.5.2.2) 1.06 μ laser

If we use an identical laser gain engine as the 1.32 μ laser, we find the following pulse energies under similar conditions

TABLE 3

Rep Rate	**Single Head 43 nm@ 500 Hz**	**Single Head 21.5 nm@ 500 Hz**
500 Hz	46.2 mJ	48.2 mJ
800 Hz	42.6 mJ	47.1 mJ
1000 Hz	39.7 mJ	46.2 mJ

(3) Sum Frequency Conversion

Each Infra-red beam focused into the non-linear crystal has an intensity profile that changes with space and time. If the two laser beams are radially symmetric and travel along the optical axis of the Sum frequency converter we can write :

$$I_{1.06}(r,t) = \frac{P_{1.06}}{(2\pi)^{3/2}\sigma_{1.06}^2\tau_{1.06}} Exp[-r^2/2\sigma_{1.06}^2] \cdot Exp[-t^2/2\tau_{1.06}^2] \qquad (9)$$

$$I_{1.32}(r,t) = \frac{P_{1.32}}{(2\pi)^{3/2}\sigma_{1.32}^2\tau_{1.32}} Exp[-r^2/2\sigma_{1.32}^2] \cdot Exp[-t^2/2\tau_{1.32}^2] \qquad (10)$$

Where $P_{1.06} = E_{1.06}/(\tau_{pw} - \tau_{turnon})$
$P_{1.32} = E_{1.32}/(\tau_{pw} - \tau_{turnon})$
σ = FWHM Intensity of beam/ 2.35
τ = FWHM pulse width of the mode locked pulse/2.35
E = Energy/pulse
τ_{pw} = Pulse width of the macropulse
τ_{turnon} = Turnon time of laser

The amount of SF light produced depends on the beam profile of the IR lasers focused in the crystal, the design of the sum frequency converter and the Non-linear conversion constant of the material. The Intensity of 0.589 μ light can be written as:

$$I_{0.589}(r,t) = (1.319/0.589) \cdot I_{1.32}(r,t) \cdot JacobiSN[\alpha \cdot \sqrt{I_{1.06}(r,t)}, \gamma]^2 \qquad (11)$$

(3.2) Mode locked pulse shapes

We measured the pulse shapes and widths of the mode locked pulses from both 1.06 μ and 1.32 μ laser in July 2004 using a 1.6 GHz bandwidth and a 6 GHz sampling oscilloscope . Representative traces are shown in photograph 2. There was no noticeable change in shape as a function of position within the macropulse.

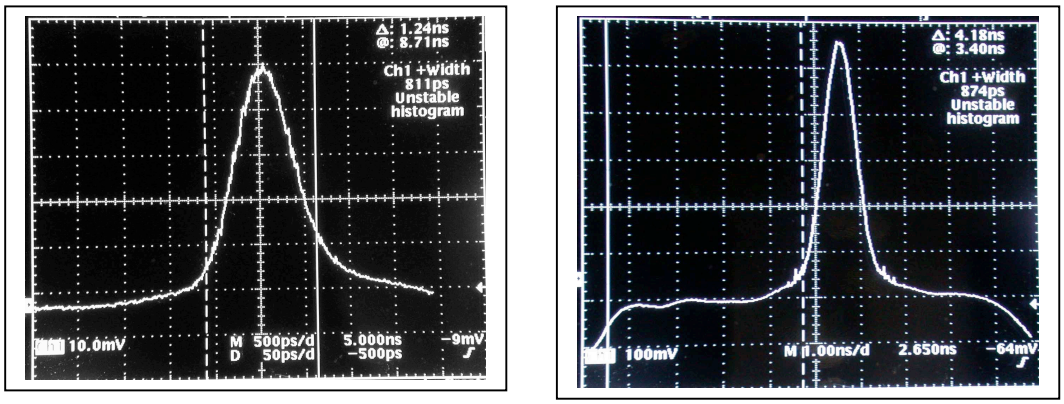

Photograph 2 : Mode Lock pulses of 1.06 μ laser (left) and 1.32 μ laser (right). Note 1.32 μ horizontal scale is twice that of the 1.06 μ laser.

These traces have been fitted with a pair of Gaussians to capture the core and halo of the pulse shape. This data is shown in figure 15. .

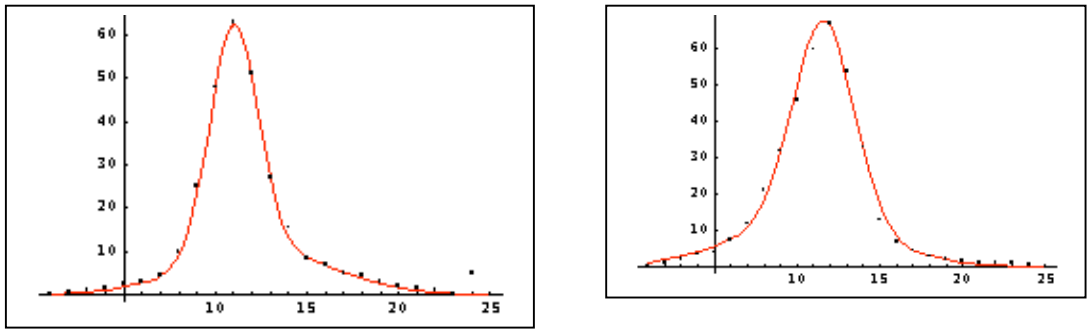

Figure 15 : *Gaussian fit to 1.06 μ (left) and 1.32 μ (right) laser mode locked pulses.*

When these measurements were made, 75% of the energy of the 1.06 μ laser was contained within a Gaussian of FWHM 0.71 nsec; 79% of the energy of the 1.32 μ laser was contained within a Gaussian of FWHM 0.94 nsec. Substantial improvements have been made to the mode locking process and we now believe that about 90% of the total energy in the mode locked pulses is contained within these Gaussian profiles.

The pulses shown in figure 15 are broadened by the response of the photodiode. The rise time of the photodiodes is 0.25 nsec and the pulse width should be about twice the rise time. This suggests deconvolved pulsewidths of 0.5 nsec for the 1.06 μ laser and 0.8 nsec for the 1.32 m laser. We have recently measured the convolution of the two IR pulses by recording the power in 0.59μ light as a function of phase difference between the two AOM drive signals. The Intensity of yellow light as a function of phase of the

mode locked pulses is shown in figure 16, together with a Gaussian profile of 0.916 nsec FWHM. The convolution pulsewidth for a pulse of 0.5 nsec and 0.8 nsec is 0.94 nsec.

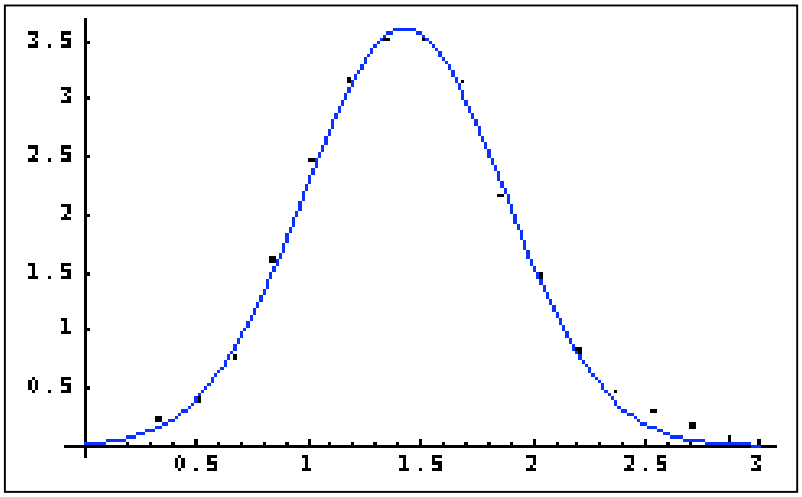

Figure 16: *Intensity of yellow light as a function of mode lock pulse phase. Horizontal scales is in nsecs. This data is well fitted with a Gaussian of FWHM 0.92 nsec.*

(3.2) SF performance of the current laser

We made measurements of the conversion power of one and three crystals under mode and non-mode locking conditions. We can determine the parameter α under known power conditions and should then in principle be able to predict the 0.589 μ light power under any other conditions. Typical characteristics of the lasers are given in table 4.

TABLE 4

Laser	Micropulse Width	Mean Power	Turn on time	$1/e^2$ OC beam radius	M^2
1.06 μ	n/a	16 Watts	32 μsec	0.090 mm	<1.2
1.06 μ	0.5 nsec	15Watts	33 μsec	0.092 mm	<1.2
1.32 μ	n/a	8.8 Watts	41 μsec	0.0625 mm	<1.2
1.32 μ	0.8 nsec	8.2 Watts	43 μsec	0.065 mm	<1.2

With 8.6 watts 1.32 μ power and 16.5 watts of 1.06 μ power, we obtained a power of 0.56 watts at 0.589 μ. Putting these values into the code gives a value of α of 0.73. Table 3 gives the measured and calculated power levels using this value of α.

TABLE 5

Mode-Locking	No. of Xtals	1.06 μ Power	η_{mode}	1.32 μ Power	η_{mode}	α	SFC Power (Measured)	SFC Power (Calculated)
No	1	16.5 Watts	n/a	8.6 Watts	n/a	0.73	0.56 Watts	0.56 Watts
Yes	1	16.0 Watts	0.9	8.2 Watts	0.9	0.73	2.7 Watts	2.7 Watts
Yes	3	14 Watts	0.9	8.2 Watts	0.9	2.19	7.8 Watts	8.4 Watts

We used the data in the first row to determine α and the data in the second row to determine the micropulse width efficiencies. The Calculated value for the third row was determined by multiplying the value of α by three (there are 3 crystals) and using measure power values.

(3.3) Increasing the power of 0.59 μ light

There are a number of ways of obtaining more SF light from the existing laser.

(3.3.1) Changing the mode locked pulse widths

There is an optimum pulse width for this laser, decreasing the mode pulsewidth increases the conversion efficiency but also increases the spectral bandwidth and this ultimately affects the photon return from the sodium layer. The relationship between bandwidth of the gain medium and mode-locked pulse width that is typical of this type of laser is

$$\Delta\nu_{FWHM} \approx \frac{0.8}{\Delta\tau_{FWHM}} \qquad (12)$$

we can predict the relative photon return from the Sodium layer . This return is shown in figure 17. This suggests that the optimum pulse width of between 0.6 and 0.8 nsec FWHM. This data can be misleading since it is quite possible for the IR lasers to "chirp" during the mode-locked pulse, indeed we observed such chirping in the original laser. This chirping is related to the AOM and etalons and can be removed by careful adjustment. The FWHM bandwidth of the MIT/LL laser was 0.9 GHz when suitable adjustments had been made.

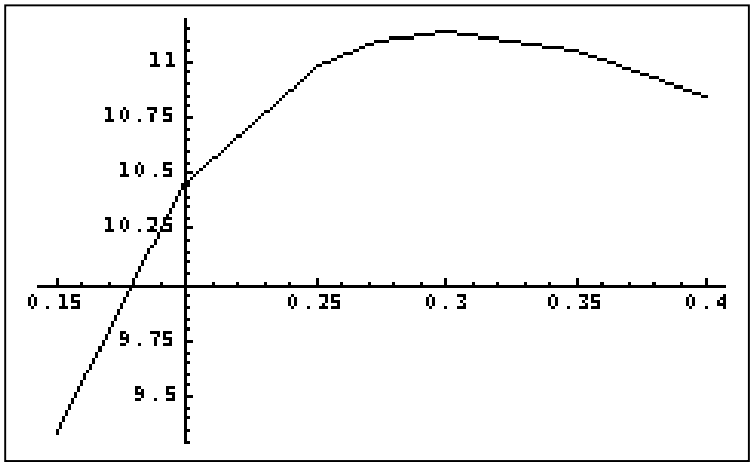

Figure 17: *Signal return as a function of 1.32 μ and 1.06 μ laser mode locked pulsewidth (standard deviation) in nsec.*

To see how accurately we should match the pulse widths we have plotted the yellow light power against the ratio of the FWHM of the 1.06 μ to 1.32μ laser mode pulsewidths constrained so that they produce the same 0.59 μ pulsewidth.

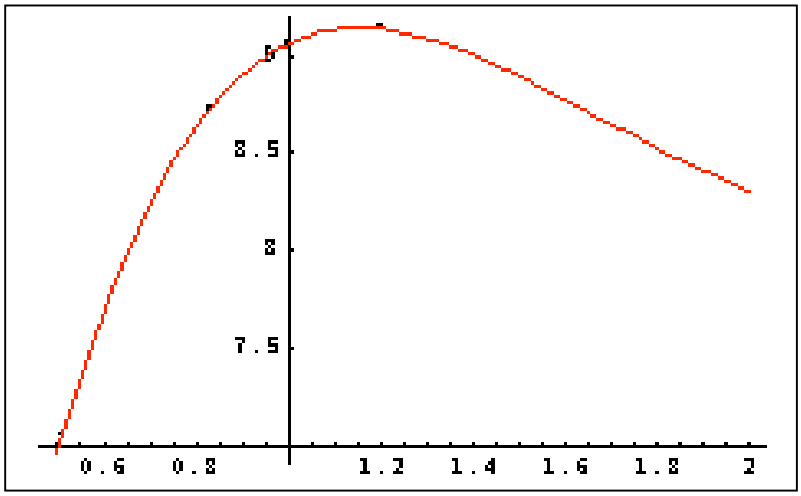

Figure 18: *The power in yellow light in the current laser configuration changing the ratio of mode locked pulsewidth of the 1.06 to 1.32 μ laser subject to the constraint that the sum frequency pulse length is fixed. The ratio is given in the horizontal axis.*

This figure shows us that the performance of the laser is not very sensitive to the ratio of the pulse lengths but that, if anything, the pulse length of the 1.32 μ laser should be shorter than that of the 1.06 μ laser (at present it is longer); this is because the 1.06 μ laser typically is producing more photons/sec than the 1.32 μ laser. According to the

code, if the pulses widths of both lasers were 0.6 nsec FWHM the SFC power would be increased from 8.38 to 9.83 watts, a significant increase of 15%.

(2.3.2) Increasing power levels

Because we are using Gaussian Intensity and pulse profiles, the SF power increases with 1.06 m power beyond the point at which the photon intensities are equal. At high powers, the radial profile distorts but the total power increases. This effect is shown in figure 19, which shows the predicted yellow light power as a function of 1.06 and 1.32 μ powers and figures 20 and 21, which show the radial profiles.

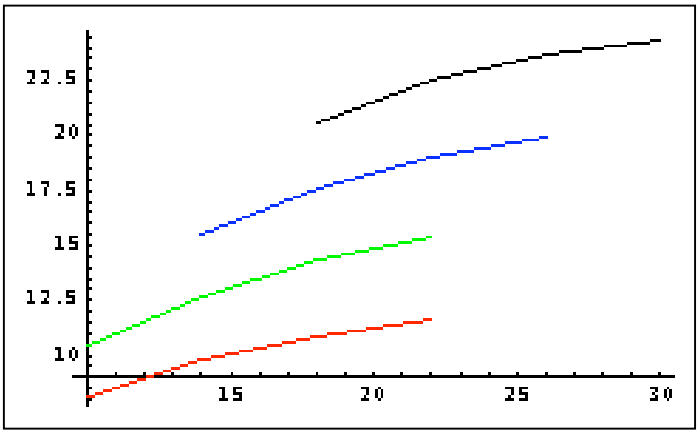

***Figure 19**: Calculated laser power @ 0.59 μ in watts as a function of 1.06 power in watts*
7.5 watts 1.32 μ power (Red), 10 watts 1.32 μ power (Green),
12.5 watts 1.32 μ power (Blue), 15 watts 1.32 μ power (Black)

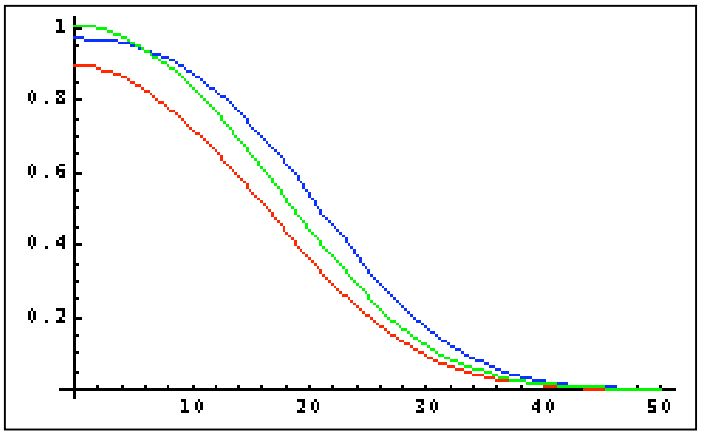

***Figure 20:** Radial profiles of sodium beam for 7.5 watts 1.32μ laser, equal pulsewidth of 0.273 ns s.d.*
Red 10 watts 1.06 μ power, Green 14 watts 1.06 μ power
Blue 22 watts 1.06 μ power

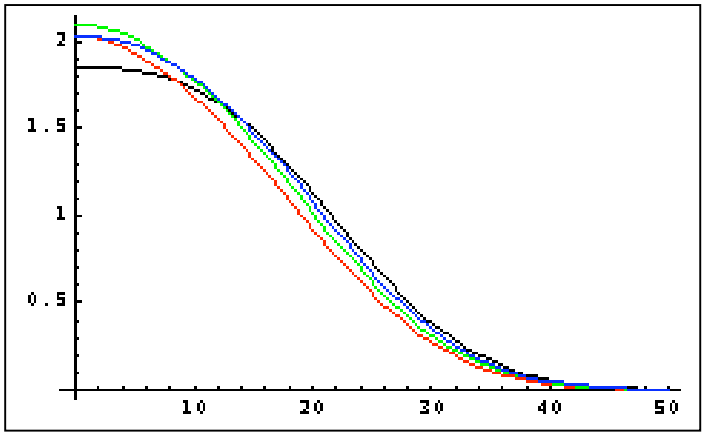

Figure 21*: Radial profiles of sodium beam for 15 watts 1.32μ laser, equal pulsewidth of 0.273 ns s.d.*

Red 18 watts 1.06 μ power, Green22 watts 1.06 μ power
Blue 26 watts 1.06 μ power, Black 30 watts 1.06 μ power

This slightly increases the diffraction limited spot size, causing a small fraction of the light to be scattered into an Airy disk. We discuss the consequences of this effect in the next section.

(2.3.3) Use of PPSLT

Pulse widths and power levels attained by CTI have recently been published enabling us to make some prediction for the power levels that might be obtained with our laser using the same material

The CTI laser produced 16 watts of 0.589 μ power with 22.3 watts of 1.06 μ power and 14.8 watts of 1.32μ power. Pulse train was CW with mode locked pulses 0.60 nsec (1.06 μ laser) and 0.51 nsec (1.32 μ laser). Putting these number into our code gives $\alpha = 3.3$. We have then calculated the power under similar drive conditions to those provided by our current laser (non-mode locked and mode locked #1) and mode-locked with a 1.06 μ power chosen to produce the same number of photons as the 1.32 μ laser.

TABLE 6

Current laser	1.06 μ Power	1.32 μ Power	LBO Power	PPSLT Power
Non-mode locked	16 Watts	8.4 Watts	3.0 Watts	7.4 Watts
Mode locked #1	14 Watts	8.2 Watts	8.2 Watts	8.6 Watts
Mode locked #2	10.25 Watts	8.2 Watts	7.8 Watts	9.2 Watts

This table shows that PPSLT may produce significant extra power compared to LBO, especially for the non-mode locked case. When the lasers are mode locked, substantial back conversion occurs in the SF process as can be seen in Figure 22 for the current laser

(red). If we match the pulsewidths and reduce the 1.06 μ power to 12 watts, we obtain more power and a much better spot.

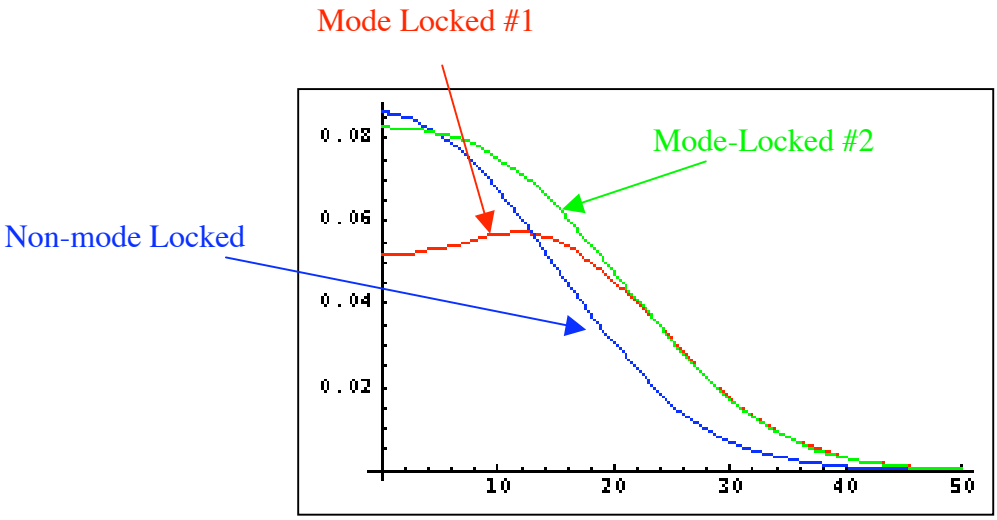

Figure 22: *Calculated radial profiles of SF light using Current laser and PSI PPSLT material*

The mode-locked SF radial profiles look highly distorted. The determine their far field pattern we calculated the square of the Fourier transform of the amplitude these profiles:

$$I(\alpha) = \left(\int_0^{50} 2\pi \cdot r \cdot \sqrt{i(r)} \cdot J_0[0.1 \cdot \alpha \cdot r] \cdot dr \right)^2 \qquad (13)$$

The resulting far-field patterns are shown in figure 23. The red and green curves are for the mode locked SF output;also shown is the profile for a Gaussain scaled to match the two mode-locked curves. Evidental we can have considerable non-linearity in the SF profile before we start to decrease the performance of the AO system.

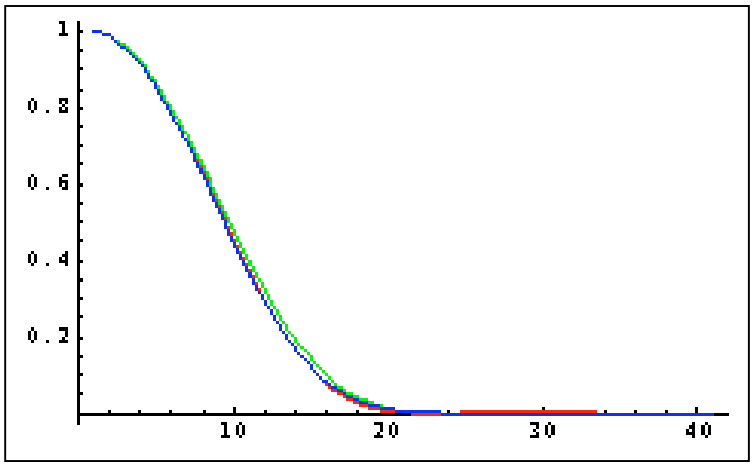

Figure 23: Far field Intensity patterns for the two mode-locked cases in figure 22. The blue curve represents a Gaussian profile for comparison.

(2.3.4) Predicted power levels of upgrades.

We are now in a position to be able to predict 0.59 μ power levels for the next generation of lasers. These are provided in the following tables . In Table 5 I have given the predicted output powers for a single and double head 1.32 μ laser with the similar performance and output couplers as the current laser but assuming that we have more powerful diode laser drive amplifiers. It may be necessary to cool the laser heads to about 10 ^{0}C -15 ^{0} C to reduce the temperature shifts of the Gain profile (3 GHz /^{o} C). The laser head is on a separate cooling line to allow for this possibility. In the summer, we may need to control the head temperature using a temperature sensor located on the head of the laser head to avoid condensation on the optics and/or diode lasers.

TABLE 7

Freq (Hz)	1.32 μ Power (W)	1.32μ Turn-on (μs)	1.06 μ Power (W)	1.06μ Turn-on (μs)	SFC Power (W)
500	8.9	42	19.6	22	9.48
800	12.5	46	28.8	23	13.2
1000	13.8	49	33.4	24	14.5

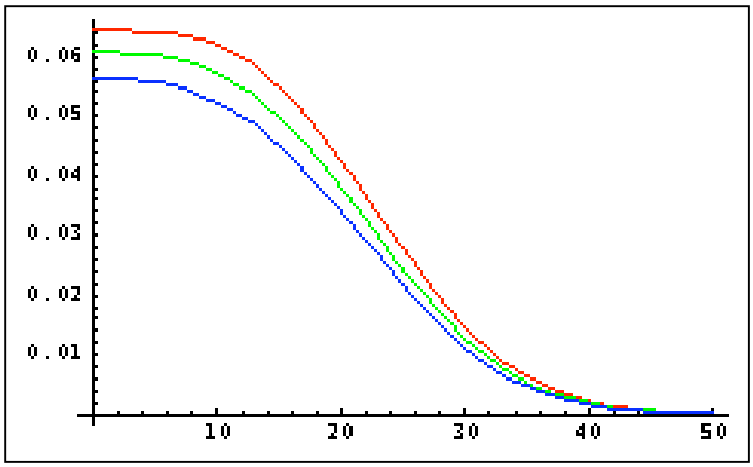

Figure 24: *SF Intensity profiles with current drive laser performance 500 Hz (red), 800 Hz (green), 1000 Hz, (blue)*

We have seen that some improvement can be made in the output power by reducing the reflectivity of the output coupler and matching the pulsewidths and these are given in table 8. We have assumed that:

(1) we can improve the output power of the 1.32 μ laser by 15% using an Output Coupler with a transmission of 0.54 for the 1.32 μ laser and 0.3 μ for the 1.06 μ laser. This increases the output power but may make the lasers more sensitive to back-scattered light from the SFC. This problem can be solved, at a sacrifice of 10% less power/laser, by using optical isolators.

(2)we can match the mode-locked pulses to be 0.6 nsec FWHM in both lasers

TABLE 8

Freq (Hz)	1.32 μ Power (W)	1.32μ Turn-on (μs)	1.06 μ Power (W)	1.06μ Turn-on (μs)	SFC Power (W)
500	10.7	46	22.1	23	14.1
800	15.1	50	33.6	24	19.8
1000	16.9	53	40.2	25	22.0

We have calculated the SF power for the final configuration of the laser in which two heads are used. We have chosen to drive each head at a slightly lower power (1500 watts peak power/head) and assume that we can match the mode-locked pulses to 0.6 nsec FWHM.

TABLE 9

Freq (Hz)	1.32 μ Power (W)	1.32μ Turn-on (μs)	1.06 μ Power (W)	1.06μ Turn-on (μs)	SFC Power (W)
500	19.6	38	22.1	23	24.9
800	24.0	44	33.6	24	30.8
1000	24.0	50	40.2	25	30.9

The increased thermal distortion arising from the use of two heads has meant that we get no increase in power going from 800 Hz to 1000 Hz either for the 1.32 μ or SF. Note also that we are underpowered with the 1.06 μ laser and may need a second head for this laser.

(2.4) Optimizing α

The PPSLT material supplied to CTI works very well for non-mode applications but saturates for pulsed mode-locked lasers. This is because,JacobiSN[β,γ] is periodic for $\gamma \neq 1$ and for any values of power and pulsewidth there is an optimum β . Figure 25 shows the SF power in watts as a function of α for a laser operating at 800 Hz with a 1.32 μ power of 24 watts and a 1.06 μ power of 33.6 watts (see Table 9) . The red curve is for mode locked operation, the blue for non mode locked. The SF intensity profiles look very

different for different values of α , although we have seen that the far-field pattern is not effected by the core of the profiles. We show the SF profiles for α = 2.5, 3.0 and 3.5 in figure 26.

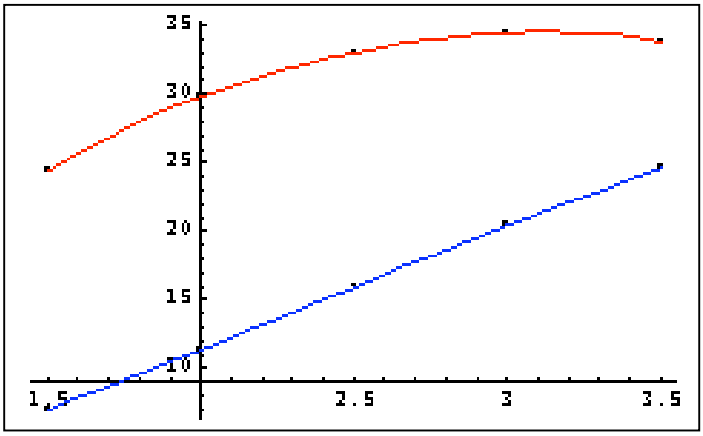

Figure 25: *Calculated SF power for 800 Hz operation in Table 9.*
Power is vertical in Watts, α is horizontal axis
Red is mode locked with 0.6 nec pulse
Blue is non-mode locked

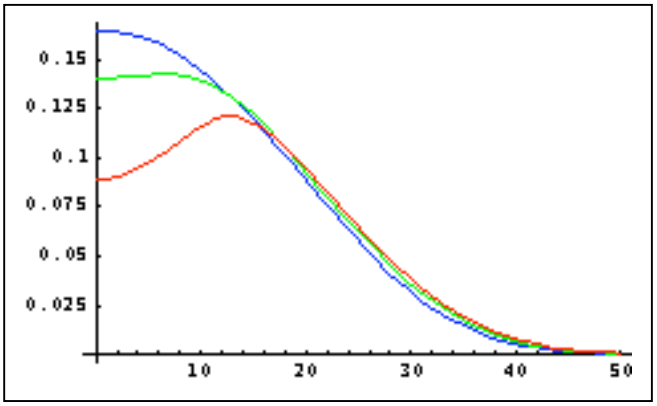

Figure 26: *Calculated SF profiles for mode-locked pulses with α = 2.5 (blue),3.0 (green) and 3.5 (red)*